2015 Project Report
Ductile fracture – Insights into the role of pore-fluid pressure on fault behavior in the lower crust
Greg Hirth

Summary

To understand the physics of crustal faulting near the brittle-ductile transition, we conducted a microstructural study on experimentally deformed quartz sandstones deformed at high pressure and temperature. Using quantitative microstructural data, we address: (1) how the relative contribution of grain-scale deformation mechanisms vary from brittle faulting to semibrittle faulting (ductile shear fracture) with changing deformation conditions; and (2) whether interactions of tensile or shear microfractures govern shear localization within these regimes. Our analysis of energy partitioning suggests that the deformation (plastic energy) prior to shear localization in both brittle faulting and semibrittle faulting regimes is accommodated primarily by grain-scale brittle mechanisms. Our analysis also indicates that the relative importance of tensile and shear microfracture and grain crushing remains similar over a wide range of the PT conditions. On the basis of characterizing the ratios of fracture spacing to length, we conclude that the interaction of mm-scale intergranular shear fractures is the primary mechanism of macroscopic fault formation in both brittle and semibrittle faulting within our granular rock samples.

Energetics of the brittle-semibrittle transition

Our microstructural observations indicate that the deformation prior to shear localization in both brittle faulting and semibrittle faulting regimes is accommodated primarily by grain-scale brittle mechanisms (Figure 1b). Nonetheless, some features of our experiments, as well as previous TEM studies of experimentally deformed quartzite at similar conditions [Mainprice and Paterson, 1984], suggest involvement of dislocation glide in the semi-brittle regime. To constrain the relative importance of brittle vs. crystal plastic mechanisms, we estimate the ratio of brittle to plastic energies, U_B/U_P. In so doing, we also assess how the relative importance of various brittle mechanisms varies across the brittle-semi-brittle transition. The total plastic energy (input) per unit volume U_P is approximated by [Edmond and Paterson, 1972; Fredrich et al., 1989]:

$$U_P \cong \int \sigma_d \, \mathrm{d}\varepsilon_p + (P_C - P_f)\,\Delta\phi \qquad (1)$$

where ε_p and $\Delta\phi$ are the axial plastic strain and porosity change. The first term on the RHS is calculated by integrating the area under the σ_d-ε_a curve to the peak stress (Figure 1a), where the onset of macroscopic fault was observed to occur in both regimes. At T ≤300°C, U_P is small and relatively constant (7-10 MJ/m^3) at pressure differences ΔP (confining pressure – pore pressure) = 75 to 150 MPa. In contrast, at 900 °C, U_P increases from 4 to 51 MJ/m^3 with increasing ΔP from 50 to 175 MPa – the ΔP range over which the brittle-semibrittle transition is observed.

For brittle energy (U_B), we consider surface (U_S) and frictional (U_F) energies as energy sinks. Microstructural observations indicate that U_S arises from tensile fractures (Figure 1c) and comminuted grains along mm-scale shear fractures and crushed zones (Figure 1b). Each component of U_S is quantified using the relationship:

$$U_S = 2\, S_V \gamma \tag{2}$$

where, S_V and γ are the crack surface area per volume and specific surface energy [Wong, 1982]; γ = 2.5 J/m^2 [Atkinson, 1984]. S_V can be estimated, for tensile cracks, from the fracture density observed [cf. Moore and Lockner, 1995], and, for comminuted grains, from the relationship [e.g., Pabst and Gregorova, 2007]:

$$S_V = \sum_i N_i^{\frac{3}{2}} \pi\, {d_i}^2 f \tag{3}$$

where f is the volume fraction of comminuted grains in a sample. The volume fraction of comminuted grains is estimated from multiplying the fracture density and average thickness of shear fractures, and point-counting the area fraction of crushed zones in gridded micrographs, respectively. A first order estimate for U_F is provided by:

$$U_f = \int_0^{\delta} \tau(\delta)\, d\delta\, \rho_s \tag{4}$$

where τ ($= \sigma_d \sin\theta$), δ, ρ_s, and θ are the shear stress and displacement (<5 to 30 μm) along, the density and the angles with respect to σ_1 (30-50°) of shear fractures. Because distributed shear fractures are observed just after yielding, we assume $\sigma_d = \sigma_y$ at $\delta = 0$ and $\sigma_d = \sigma_{peak}$ at $\delta = \delta_{observed}$.

Our analysis shows that U_B increases with increasing PT in a manner similar to that of U_P. At ≤300°C both U_S and U_F are small and relatively constant at ΔP up to

150 MPa, whereas at 900 °C they increase considerably with ΔP (Figures 2a and 2c). The ratios U_S/U_P and U_F/U_P range 4-12 and 70-240%, respectively. Both U_S and U_F scale linearly with U_P; the slope of U_S/U_P and U_F/U_P is determined to be ~5 and 166%, respectively (Figures 2b and 2d), which represents the average fraction of each sink to the energy budget. These calculations suggest that the total energy input (U_P) can be accounted for by the brittle energy, i.e., the sum of U_S and U_F. Similarly, the ratio of each component of U_S over U_P remains constant at all conditions tested. Thus, these results suggest that deformation in both the brittle faulting and semibrittle regimes is accommodated via grain-scale brittle mechanisms with little contribution from crystal plastic mechanisms.

Our 900°C vented and ≤300°C tests show similar strengths at the same ΔP, yet the high T samples exhibit much more ductility (Figure 1a). Together with the calculations in the energetics of deformation, these observations suggest that the suppression of strain localization arises from factors other than a change in grain-scale deformation mechanism. We conclude that the primary role of temperature is to enhance sub-critical crack growth, similar to the findings from previous studies [e.g., Katz and Reches, 2004; Chester et al., 2005; Brantut et al., 2013].

Microfracture interaction in brittle and semibrittle faulting

Fracture mechanics models of multiple cracks suggest that the interaction of nearby cracks becomes increasingly significant when the ratio of fracture spacing / length (S/L) is small [e.g., Segall and Pollard, 1980]. For fractures with a strong preferred orientation (i.e., parallel fractures), significant interaction is expected at S/L < 2, regardless of whether fractures are collinear or offset (such as observed for the tensile and shear microfractures in our samples) [Rooke and Cartwright, 1974]. By characterizing S/L ratios over a range of length scales, we assess (1) whether the interaction of tensile or shear microfracture governs shear localization in our granular aggregate samples, and (2) how the mechanism of shear localization varies from brittle to semibrittle faulting. S/L ratios are estimated using the relationship [e.g., Katz and Reches, 2004]:

$$S/L = (A/NL^2)^{0.5} \quad (5)$$

where A and N are the measurement area and the number of microfractures for each fracture size bin; L and N are determined from digitized maps of tensile (Figure 1c) and shear (not shown) microfractures.

Our analysis suggests that, for both brittle and semibrittle faulting, the interaction of tensile microfractures is not significant because the minimum S/L (= 4.1 and 2.6

for the former and latter regimes, respectively) is greater than the critical S/L of ~2 (Figures 3a and 3c). In both regimes, our results show that the majority of tensile microfractures are shorter than the average grain size (i.e., intragranular), and that the fracture lengths showing the minimum S/L are two orders of magnitude smaller than the sample size. Based on these constraints, we infer that in porous rocks the length scale of tensile stress field (which generates along Hertzian contacts) is restricted within grains, suppressing the interaction and linkage of tensile cracks.

We conclude that the interaction of intergranular shear microfractures is the primary mechanism of shear localization in both deformation regimes. Many shear microfractures - including those showing the minimum S/L - have lengths of 1-3 mm, which are conformable with the sample size (20 mm).

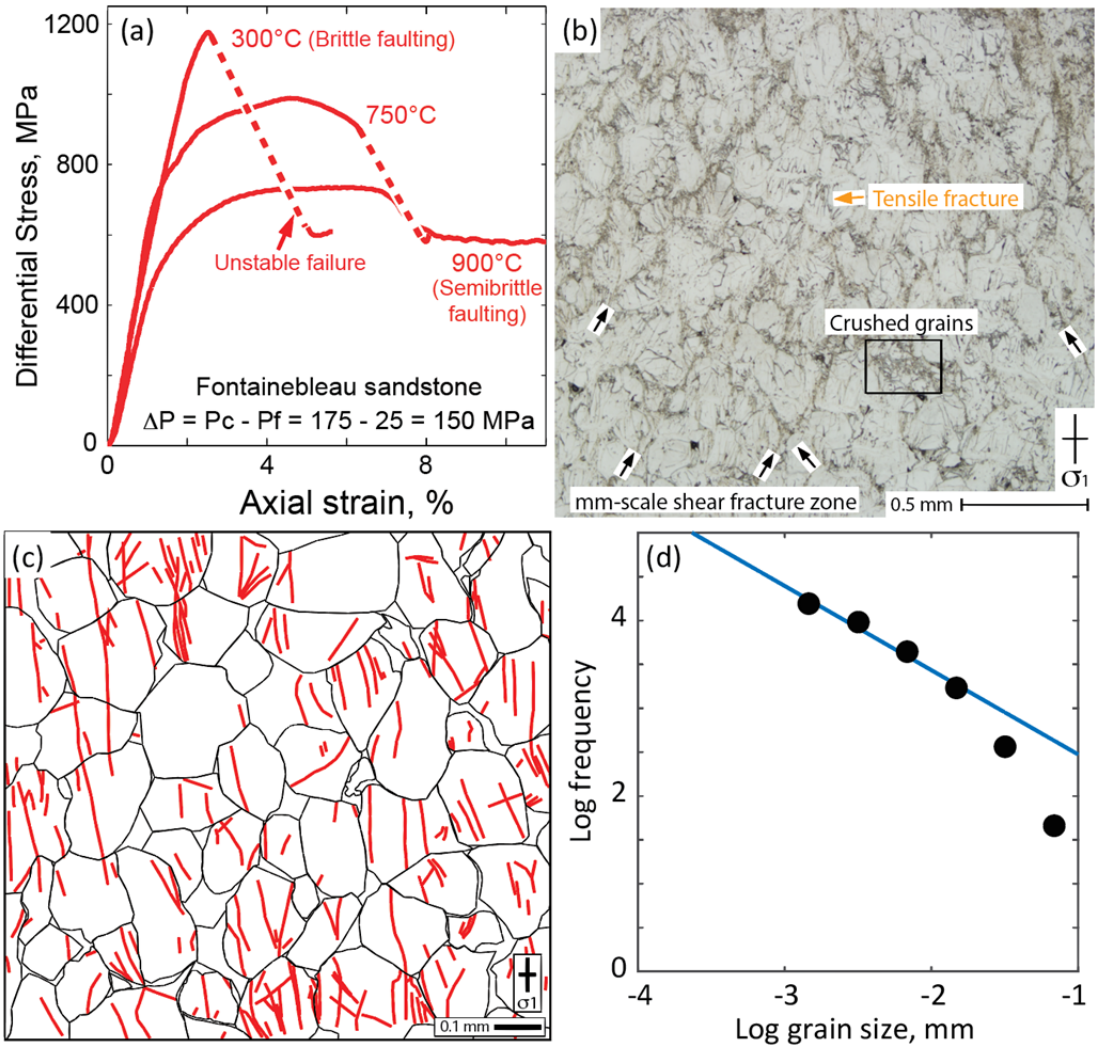

Figure 1. (a) Differential stress vs. axial strain plot showing a transition from brittle faulting to semibrittle faulting (ductile shear fracture) with increasing temperature. (b) Photomicrograph (reflected light) of a sample deformed in the semibrittle regime at 900°C and ΔP = 150 MPa, showing distributed cataclasis (e.g., intragranular tensile fractures, mm-scale intergranular shear fractures, and zones of crushed grains) in a region away from the macroscopic fault. (c) A map of tensile microfractures, which was used to determine fracture density in calculating surface energy (cf. Figure 2) and characterize fracture geometrical configuration (cf. Figure 3). This example is from a sample deformed in the brittle faulting regime at 20°C and ΔP = 75 MPa. (d) Particle size distribution in a shear fracture zone, which was used to estimate the total surface area and surface energy in the zone. This example is from a sample deformed in the semibrittle regime at 900°C and ΔP = 150 MPa.

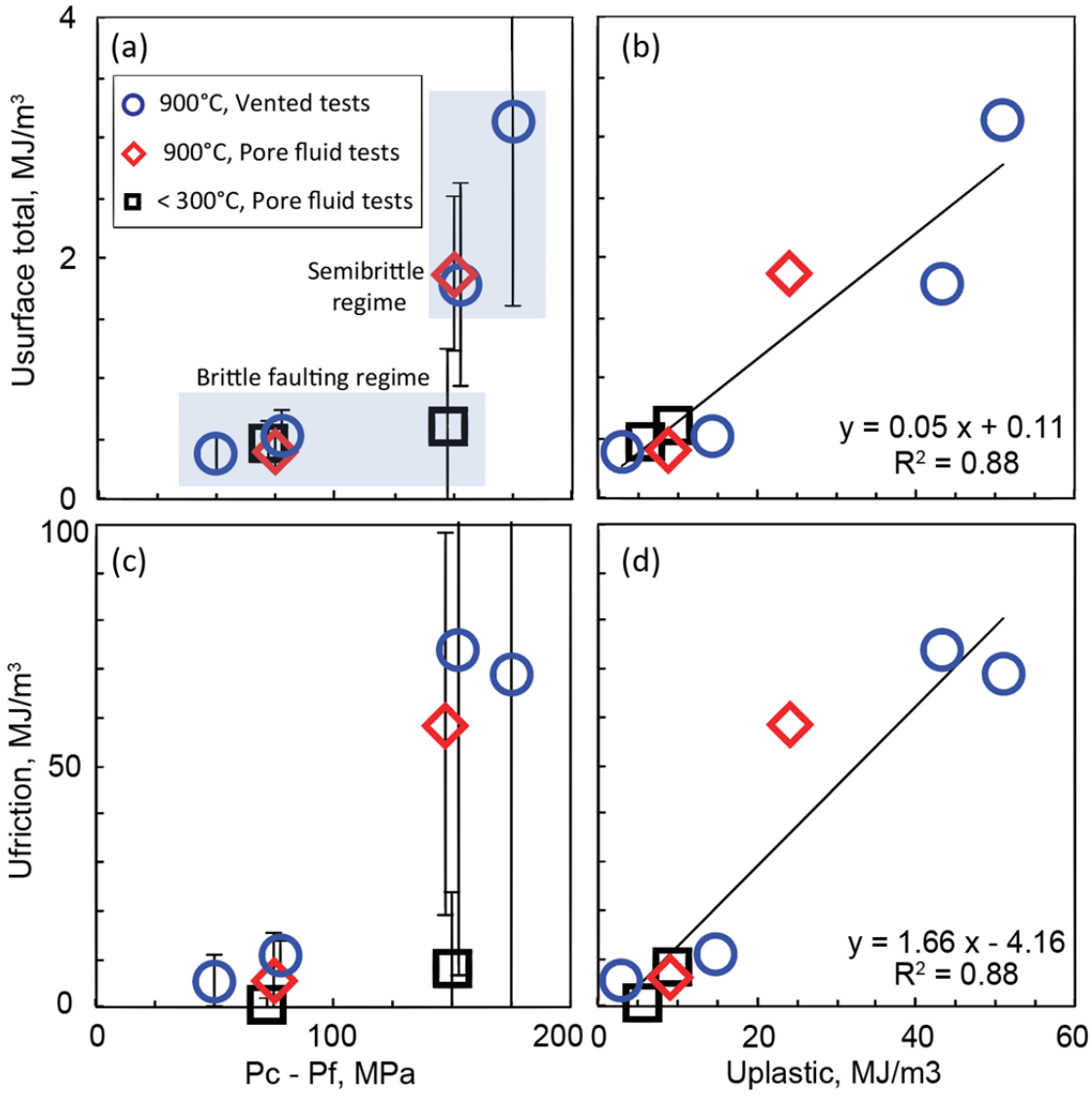

Figure 2. Energetics of the brittle-semibrittle transition. Total surface energy vs. (a) effective pressure and (b) plastic energy (input). Frictional energy vs. (c) effective pressure and (d) plastic energy. For both total Us and U_F, the brittle faulting regime shows low values, whereas the semibrittle regime shows high values. As a result, both energies scale with Up, in which the slopes of 0.05 and 1.66 against Up indicate that, for both regimes, only ~5% of energy is expended in producing microstructures, and the rest (~95%) is dissipated as heat.

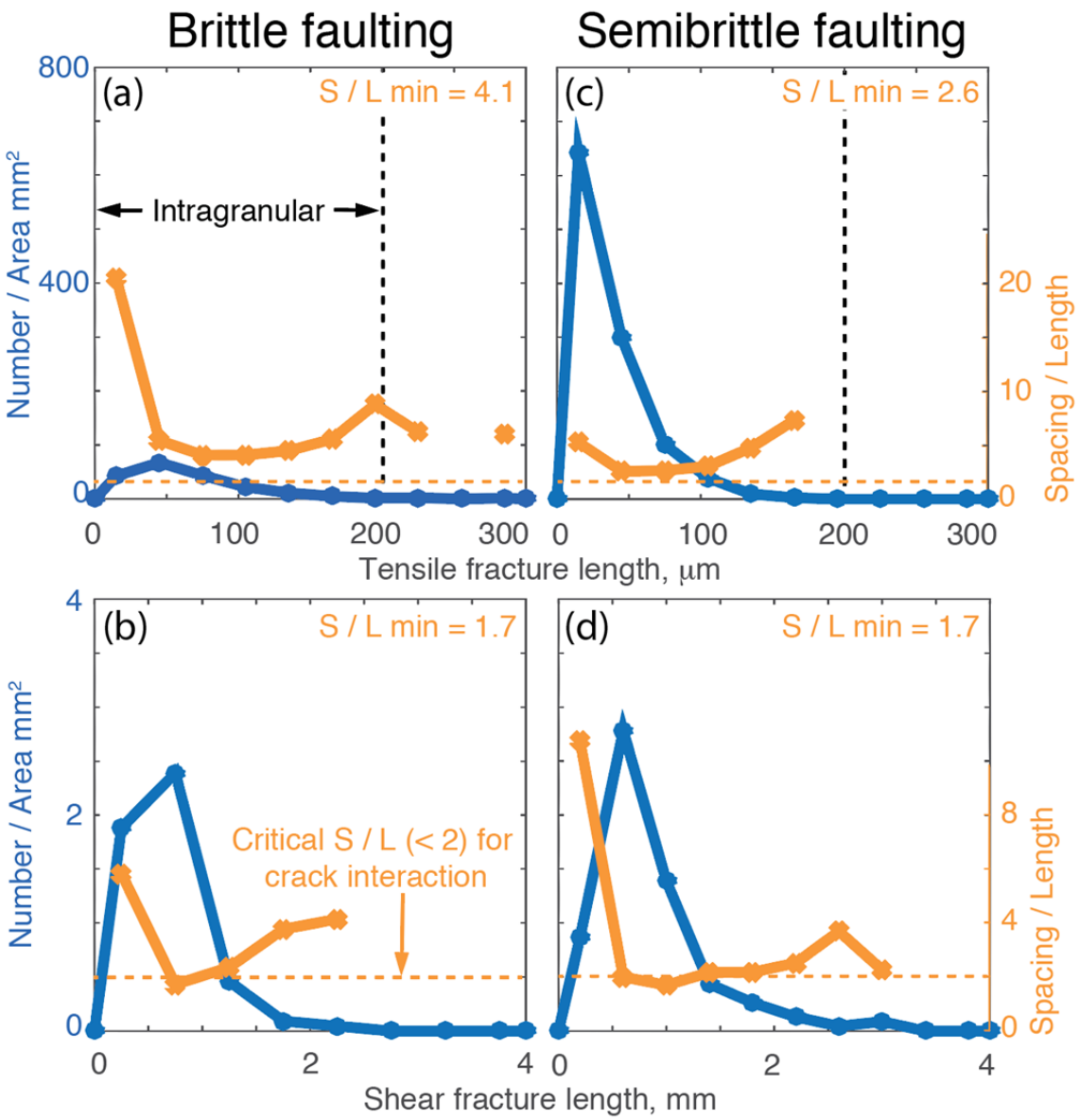

Figure 3. The number density and spacing / length ratio of microfractures in regions away from the macroscopic fault as a function of fracture size. (a) Tensile and (b) shear fractures in the brittle faulting regime (sample deformed at 20°C, ΔP = 75 MPa, ε_p = 1%). (c) Tensile and (b) shear fractures in the semibrittle faulting regime (900°C, ΔP = 150 MPa, ε_p = 5%). For both regimes, tensile fractures show large S/L, indicating no significant crack interaction. In contrast, S/L < 2 observed for shear fractures suggests that the linkage of distributed shear fractures is the main mechanism of shear localization (macroscopic faulting) for both regimes in porous rocks.

Outreach: The results of our project are being presented during lectures for classes and during seminars at other labs, universities and meetings.

Manuscript

Kanaya, T., and Hirth, G., Effects of temperature and pore fluid pressure on deformation of porous quartz sandstone: 1. Energetics of the brittle-ductile transition, submitted, *J. Geophys. Res*.

REFERENCES

Atkinson, K. (1984), Subcritical Crack Growth in Geological Materials, *J. Geophys. Res.*, *89*(B6), 4077–4114, doi:10.1029/JB089iB06p04077.

Brantut, N., M. J. Heap, P. G. Meredith, and P. Baud (2013), Time-dependent cracking and brittle creep in crustal rocks: A review, *J. Struct. Geol.*, *52*(1), 17–43, doi:10.1016/j.jsg.2013.03.007.

Cartwright, D. J., and D. P. Rooke (1974), Approximate stress intensity factors compounded from known solutions, *Eng. Fract. Mech.*, *6*(3), 563–571, doi:10.1016/0013-7944(74)90013-7.

Chester, J. S., F. M. Chester, and A. K. Kronenberg (2005), Fracture surface energy of the Punchbowl fault, San Andreas system., *Nature*, *437*(7055), 133–136, doi:10.1038/nature03942.

Fredrich, J. T., B. Evans, and T.-F. Wong (1989), Micromechanics of the Brittle to Plastic Transition in Carrara Marble, *J. Geophys. Res.*, *94*(B4), 4129–4145, doi:10.1029/JB094iB04p04129.

Katz, O., and Z. Reches (2004), Microfracturing, damage, and failure of brittle granites, *J. Geophys. Res.*, *109*(B1), 1–13, doi:10.1029/2002JB001961.

Mainprice, D., and M. Paterson (1984), Experimental studies of the role of water in the plasticity of quartzites, *J. Geophys. Res.*

Moore, D. E., and D. A. Lockner (1995), The role of microcracking in shear-fracture propagation in granite, *J. Struct. Geol.*, *17*(1), doi:10.1016/0191-8141(94)E0018-T.

Pabst, W., and E. Gregorova (2007), Characterization of particles and particle systems, *ICT Prague*, 1–122.

Paterson, M. S., and J. M. Edmond (1972), Deformation of graphite at high pressures, *Carbon N. Y.*, *10*(1), 29–34, doi:10.1016/0008-6223(72)90006-1.

Segall, P., and D. D. Pollard (1980), Mechanics of discontinuous faults, *J. Geophys. Res.*, *85*(B8), 4337, doi:10.1029/JB085iB08p04337.

Wong, T. (1982), Shear fracture energy of Westerly granite from post□failure behavior, *J. Geophys. Res.*